TECHNIUM

Technium Vol. 2, Issue 6 pp.41-60 (2020)
ISSN: 2668-778X
www.techniumscience.com

Optimization of sensorless sliding mode control of an induction motor taking into account magnetic saturation effects

Eric Duckler Kenmoe Fankem*, Hiswe Fatamou, Alix Dountio Tchioffo, Joseph Yves Effa

Department of Physics, Faculty of Science, The University of Ngaoundéré, P.O. Box 454 Ngaoundere-Cameroon

Corresponding author: fankeme@yahoo.fr

Abstract. This paper presents the optimization of sensorless sliding-mode control for induction motor, considering magnetic saturation effects. A five-order sliding-mode observers and estimators are elaborated to replace the sensors of an induction motor. The proposal is based on double optimization of sensorless sliding mode control of an induction motor in the point of view of dynamic and energetic performances. In order to obtain better performances of the proposed control method, Particle Swarm Optimization (PSO) algorithm is used notably to determine the optimal gains of the observers as well as the optimal parameters of the regulators. Regarding the energetic optimization, the reference of the rotor flux is generated using another developed algorithm that permits us to dynamically determine the optimal rotor flux for each given value of motor load and speed. As results, sensorless sliding mode control takes into account all operating ranges of the machine from very low speeds, low speeds, to high speed with or without load. Numerical simulations are carried out each time to confirm theoretical predictions.

Keywords. Particle swarm optimization, Magnetic saturation, Sensorless control of an induction motor, Sliding mode control, interconnected sliding mode observers.

1. Introduction

Traditionally, AC motors are used in fixed speed applications. However, in order to increase their energy efficiency and improve their control process, manufacturers are increasingly using variable speed AC motors. Thus, the use of the asynchronous motor in variable speed applications became natural. The asynchronous motor is distinguished from the DC motor by its mass power, its superior speed, its robustness and its low cost. The absence of brushes and mechanical collector allows it to be the privileged motor in many areas such as aerospace, chemistry, medicine where a less frequent maintenance is required. However, these advantages have been inhibited a long time by the complexity of it control due to the fact that the analytic model of the induction motor is strongly nonlinear and parameters of the motor are uncertain.

The induction drive control techniques such as Field Orientation Control (FOC) and Direct Torque Control (DTC) are well treated in the literature [3, 4]. However, the parametric variations in the above-mentioned methods affect deeply their dynamic performances and even the stability of practical implementation. One of the mains reasons of parametric deviation is the carelessness of the magnetic saturation phenomenon [12, 19]. To solve this problem, some authors [6, 13] have considered magnetic saturation but their control strategies were proposed without observers.

Among different control strategies, nonlinear technique is one of the effective methods for induction motor drive control because of its ability to reject disturbance, its strong robustness to the variation of the system parameters and its simplicity to practical implementation by power electronics converters. There are many papers which reported control of induction motors using nonlinear technique [1-18]. However, the overall stability of these nonlinear controllers is proved using Lyapunov theory which does not ensure in spite of its global proofs of stability, optimal convergence and robustness. Indeed, Lyapunov theory only determines ranges of the gains and parameters but not their accurate values especially when one considers magnetic saturation effect. To overcome this drawback, trial by error technique is used to find approximate values of gains after a long calculation. The operations are therefore time consuming and the obtained values remain close to ideal value. [18] tried considering saturation but their nonlinear controller was developed without observers. [2] also consider magnetic saturation effect but the proposed control strategy is not validated in very low speed critical zone. [7] are the first who proposed sensorless control based on a saturated model which is validated in all operating range of the machine. Their control strategy (field-oriented control) was associated to a Luenberger type interconnected observers. Despite the good results the authors obtained, one must know that the Luenberger observers use a simple structure allowing fast convergence rates, but it depends on the accuracy of the numerical model of the system [8], which is not ideal for high-rate systems. In the same way, [20] presented a comparative study of three kinds of observers for Direct Field Oriented Controller (DFOC) of induction motor drive. They found the computational times of the Luenberger observer's and sliding mode observer to be equivalent. However, the robustness to inaccurate models and the fast-computational times make the sliding mode observer more suitable for the high-rate problem. According to [2,11] among different categories of control strategies, sliding mode controller is one of the effective practice methodologies for induction motor drive control because of its disturbance rejection, strong robustness subject to system parameter variations and uncertainties and particularly its simplicity of practical implementation by power electronics converters. It then appears that sliding mode controller associated to sliding mode observer is a popular sensorless control that is known for its robustness to inaccurate models.

In this paper, using model of induction motor drive in the stationary reference frame and considering magnetic saturation, sensorless sliding mode controller with energy optimization is introduced. The overall stability and global convergence of the system is proved by PSO algorithm. The interconnected sliding mode observers are employed in order to observe the rotor current vector, rotor speed and to estimate rotor flux.

2. Mathematical equations of induction motor with magnetic saturation

The nomenclature of the main dimensions of the machine are given below in Table 1

Table 1. Nomenclature.

Stator voltages, Rotor voltages	V_{dqs} , V_{dqr}
Stator currents, Rotor currents	i_{dqs} , i_{dqr}
Stator resistance, Rotor resistance	R_s , R_r
Stator flux, Rotor flux	φ_{dqs} , φ_{dqr}
Rotor winding self-inductance	L_r
Stator winding self-inductance	L_s
Rotor leakage self-inductance	$L_{\sigma r}$
Stator leakage self-inductance	$L_{\sigma s}$
Stator frame, electrical angular speed	ω_s, $p\Omega$
Mutual inductance	M

Technium Vol. 2, Issue 6 pp.41-60 (2020)
ISSN: 2668-778X
www.techniumscience.com

In this section, we present the global structure of the proposed sensorless control strategy as depicted in Figure 1 and electrical state equation of the saturated machine. The global structure is a combination of an inverter, induction motor, observers, estimators and dynamic generator of rotor flux reference. The inverter is a H-bridge converter operating in accordance to the very well-known Pulse Width Modulation (PWM) principle. This inverter consists of six Insulated Gate Bipolar Transistor (IGBT) with anti-parallel diodes for bidirectional power flow mode.

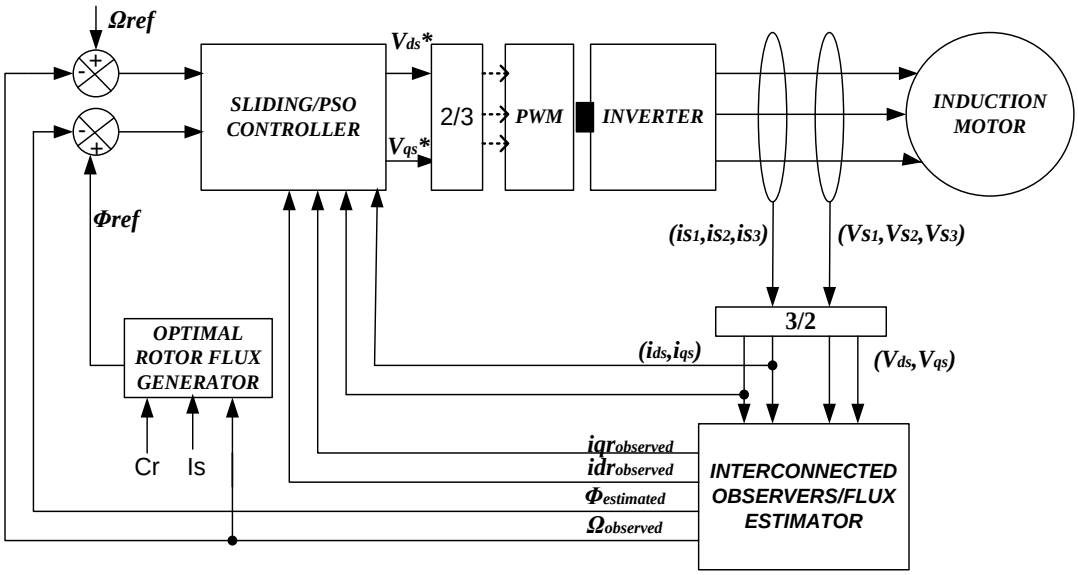

Figure 1. Global structure of the proposed sensorless control strategy

While the electrical state equations of the saturated machine modeled from a 36 kW real machine is presented as follows [16]:

$$[V]=[L]\left[\dot{I}\right]+[R][I] \tag{1}$$

Where:

$$[I]=\begin{bmatrix} i_{ds} \\ i_{qs} \\ i_{dr} \\ i_{qr} \end{bmatrix},\ \left[\dot{I}\right],\ [V]=\begin{bmatrix} V_{ds} \\ V_{qs} \\ 0 \\ 0 \end{bmatrix},\ [L]=\begin{bmatrix} L_s & 0 & M & 0 \\ 0 & L_s & 0 & M \\ M & 0 & L_r & 0 \\ 0 & M & 0 & L_r \end{bmatrix},$$

$$[R]=\begin{bmatrix} R_s & -\omega_s L_s & 0 & -\omega_s M \\ \omega_s L_s & R_s & \omega_s M & 0 \\ 0 & -(\omega_s - p\Omega)M & R_r & -(\omega_s - p\Omega)L_r \\ (\omega_s - p\Omega)M & 0 & (\omega_s - p\Omega)L_r & R_r \end{bmatrix}$$

These values are respectively matrix of stator and rotor current of the motor in dq reference, derivative matrix of stator and rotor current of the motor in dq reference, vector of stator and short-circuited rotor voltages of the machine, matrix of mutual inductance, stator and rotor winding self-inductance and combination matrix of resistances and inductances of the machine.

Equations of the electromagnetic torque as well as the dynamics of the speed of the machine are given by:

$$C_{em} = \frac{3}{2} pM(i_{dr}i_{qs} - i_{qr}i_{ds}) \tag{2}$$

$$\frac{d\Omega}{dt} = \frac{1}{J}(\frac{3}{2} pM(i_{dr}i_{qs} - i_{qr}i_{ds}) - C_r - f\Omega) \tag{3}$$

Components of magnetization currents according to dq axes can be written as:

$$i_{md} = i_{ds} + i_{dr} \tag{4}$$

$$i_{mq} = i_{qs} + i_{qr} \tag{5}$$

And the global magnetization current of the machine is given by:

$$i_m = \sqrt{i_{md}^2 + i_{mq}^2} \tag{6}$$

Considering the magnetic saturation in the modelling of the asynchronous machine is done considering that the inductances vary as a function of the magnetization current as follows [15-17] :

$$L_s(i_m) = L_{\sigma s}(i_m) + M(i_m) \tag{7}$$

$$L_r(i_m) = L_{\sigma r}(i_m) + M(i_m) \tag{8}$$

Inductances values of the machine considered in this work were determined experimentally, then approximated using polynomial functions [16] (Okoro 2004). They are given by:

$$L_{\sigma s}(i_m) = -2.6e^{-9}i_m^3 - 1.8e^{-7}i_m^2 - 4.9e^{-5}i_m + 0.38 \quad [mH] \tag{9}$$

$$L_{\sigma r}(i_m) = -8.7e^{-10}i_m^3 - 5.1e^{-8}i_m^2 - 1.6e^{-5}i_m + 0.12 \quad [mH] \tag{10}$$

$$M(i_m) = 1.2e^{-14}i_m^7 - 8.4e^{-12}i_m^6 + 2.1e^{-9}i_m^5 - 2e^{-7}i_m^4 + 6.2e^{-6}i_m^3 - 1.7e^{-4}i_m^2 + 2.9e^{-4}i_m + 8.3 \quad [mH] \tag{11}$$

3. Particle swarm optimization algorithm

We first present the PSO algorithm which is used in the next sub-section to ensure the stability and the global convergence of the observation errors to zero. PSO algorithm is part of the stochastic methods of evolutionary type with fast convergence [9, 14]. Numerous applications of this algorithm in several domains and especially in engineering show its superiority compared to the other stochastic methods like the genetic algorithm, the biogeography and the colony of ants. It is an iterative algorithm. At every step of calculation, values of the individuals are compared according to the objective function fixed, the new guides are then chosen. The flowchart of this algorithm is given in Figure 2.

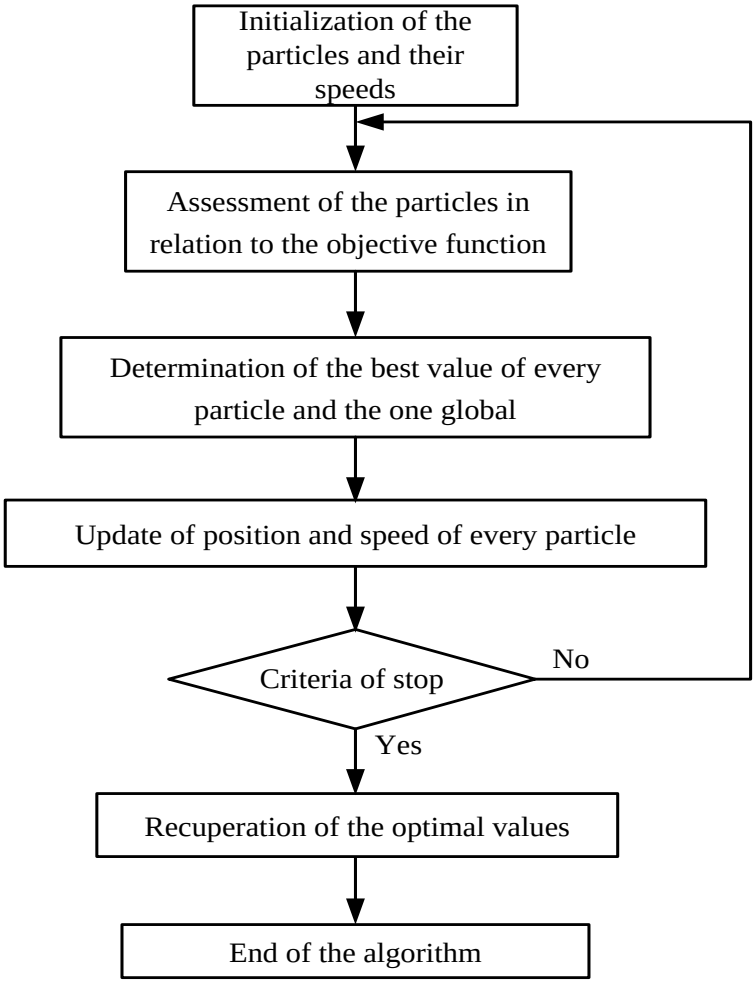

Figure 2. Flowchart of the PSO algorithm

The update of the position and the speed of every particle are done by applying the following equations:

$$\begin{cases} V_{i+1} = \gamma_1 V_i + \gamma_2 (x_{ip} - x_i) + \gamma_p (x_g - x_i) \\ x_{i+1} = x_i + V_{i+1} \end{cases} \quad (12)$$

Where $\gamma_1, \gamma_2, \gamma_3 \in [0, 1]$. x_{ip}, x_g are respectively the best position of an ith particle from the first iteration, and the best global position of the swarm.

4. Synthesis of interconnected sliding mode observers

The induction motor being saturated, we decompose the global nonlinear system into two nonlinear subsystems of small sizes in order to simplify the observer's synthesis.

The first subsystem is then given by :

$$\begin{cases} \dot{X}_1 = A_1(u, y, X_2) X_1 + g_1(u, y, X_1, \dot{X}_2) \\ y_1 = C_1 X_1 \end{cases} \quad (13)$$

With

$$A_1 = \begin{bmatrix} -\frac{R_s}{L_s(i_m)} & 0 \\ -\frac{3}{2J} pM(i_m) i_{qr} & -\frac{f}{J} \end{bmatrix}, g_1 = \begin{bmatrix} \frac{V_{ds}}{L_s(i_m)} + \omega_s i_{qs} + \frac{\omega_s M(i_m) i_{qr}}{L_s(i_m)} - \frac{M(i_m)}{L_s(i_m)} \frac{di_{dr}}{dt} \\ \frac{1}{J}(\frac{3}{2} pM(i_m) i_{dr} i_{qs} - C_r) \end{bmatrix}, C_1 = \begin{bmatrix} 1 & 0 \end{bmatrix},$$

$$X_1 = \begin{bmatrix} i_{ds} \\ \Omega \end{bmatrix}$$

And the second subsystem is given by :

$$\begin{cases} \dot{X}_2 = A_2(u, y, X_1) X_2 + g_2(u, y, X_1, \dot{X}_1, \dot{X}_2) \\ y_2 = C_2 X_2 \end{cases} \quad (14)$$

$$A_2 = \begin{bmatrix} \frac{R_s}{L_s(i_m)} & -\frac{\omega_s M(i_m)}{L_s(i_m)} & 0 \\ (\omega_s - p\Omega)\frac{M(i_m)}{L_r(i_m)} & -\frac{R_r}{L_r(i_m)} & (\omega_s - p\Omega) \\ 0 & -(\omega_s - p\Omega) & -\frac{R_r}{L_r(i_m)} \end{bmatrix}$$

$$g_2 = \begin{bmatrix} \frac{V_{qs}}{L_s(i_m)} - \omega_s i_{ds} - \frac{M(i_m)}{L_s(i_m)}\frac{di_{qr}}{dt} \\ -\frac{M(i_m)}{L_r(i_m)}\frac{di_{ds}}{dt} \\ -(\omega_s - p\Omega)\frac{M(i_m)}{L_s(i_m)} i_{ds} - \frac{M(i_m)}{L_r(i_m)}\frac{di_{qs}}{dt} \end{bmatrix}, C_2 = \begin{bmatrix} 1 & 0 & 0 \end{bmatrix}, X_2 = \begin{bmatrix} i_{qs} \\ i_{dr} \\ i_{qr} \end{bmatrix}.$$

Based on the two aforementioned subsystems, the states to be observed are therefore the rotor currents and the speed of the machine. The choice of these states justifies itself by the fact that the inductive parameters and the magnetic states (fluxes) depend exclusively of the magnetization current when one considers the magnetic saturation. The use of the dynamics of the currents is therefore logically more convenient for the synthesis of observers when the magnetic saturation is considered. The structure of the interconnected observer is thus presented in Figure 3.

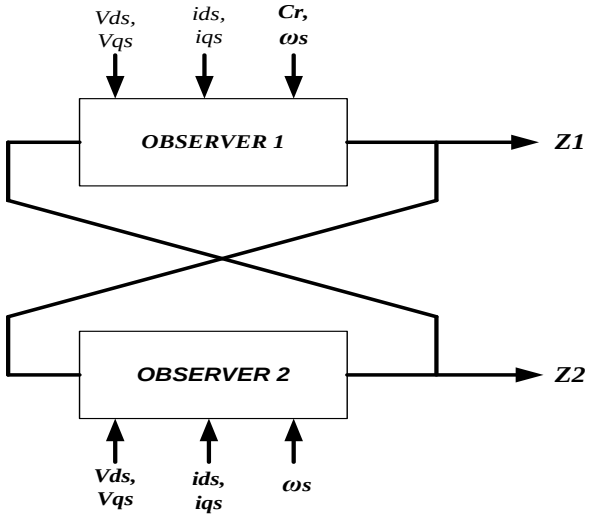

Figure 3. Structure of the interconnected observer

From Figure 3, the observers of equations (13) and (14) can be given by:

$$\begin{cases} \dot{Z}_1 = B_1(u, y, Z_2)Z_1 + h_1(u, y, Z_1, \dot{Z}_2) + [G](y_1 - \hat{y}_1) \\ \hat{y}_1 = C_1 Z_1 \end{cases} \quad (15)$$

$$\begin{cases} \dot{Z}_2 = B_2(u, y, Z_1)Z_2 + h_2(u, y, Z_1, \dot{Z}_1, \dot{Z}_2) + [K](y_2 - \hat{y}_2) \\ \hat{y}_2 = C_2 Z_2 \end{cases} \quad (16)$$

$$Z_1 = \begin{bmatrix} \$_{ds} \\ \hat{\Omega} \end{bmatrix}, Z_2 = \begin{bmatrix} \$_{qs} \\ \$_{dr} \\ \$_{qr} \end{bmatrix}, [G] = \begin{bmatrix} G_1 \\ G_2 \end{bmatrix} \text{ and } [K] = \begin{bmatrix} K_1 \\ K_2 \\ K_3 \end{bmatrix} B_1 = \begin{bmatrix} -\frac{R_s}{\hat{L}_s(i_m)} & 0 \\ -\frac{3}{2J} p \hat{M}(i_m) \$_{qr} & -\frac{f}{J} \end{bmatrix}$$

$$h_1 = \begin{bmatrix} \frac{V_{ds}}{\hat{L}_s(i_m)} + \omega_s \$_{qs} + \frac{\omega_s \hat{M}(i_m) \$_{qr}}{\hat{L}_s(i_m)} - \frac{\hat{M}(i_m)}{\hat{L}_s(i_m)} \frac{d\$_{dr}}{dt} \\ \frac{1}{J}(\frac{3}{2} p \hat{M}(i_m) \$_{dr} \$_{qs} - C_r) \end{bmatrix}$$

$$B_2 = \begin{bmatrix} \frac{R_s}{\hat{L}_s(i_m)} & -\frac{\omega_s \hat{M}(i_m)}{\hat{L}_s(i_m)} & 0 \\ (\omega_s - p\hat{\Omega})\frac{\hat{M}(i_m)}{\hat{L}_r(i_m)} & -\frac{R_r}{\hat{L}_r(i_m)} & (\omega_s - p\hat{\Omega}) \\ 0 & -(\omega_s - p\hat{\Omega}) & -\frac{R_r}{\hat{L}_r(i_m)} \end{bmatrix}$$

$$h_2 = \begin{bmatrix} \frac{V_{qs}}{\hat{L}_s(i_m)} - \omega_s \$_{ds} - \frac{\hat{M}(i_m)}{\hat{L}_s(i_m)} \frac{d\$_{qr}}{dt} \\ -\frac{\hat{M}(i_m)}{\hat{L}_r(i_m)} \frac{d\$_{ds}}{dt} \\ -(\omega_s - p\hat{\Omega})\frac{\hat{M}(i_m)}{\hat{L}_s(i_m)} \$_{ds} - \frac{\hat{M}(i_m)}{\hat{L}_r(i_m)} \frac{d\$_{qs}}{dt} \end{bmatrix}$$

Let's define the matrices of errors of the two interconnected observers such as:

$$[e_1] = X_1 - Z_1 = \begin{bmatrix} i_{ds} - \$_{ds} \\ \Omega - \hat{\Omega} \end{bmatrix} \quad (17)$$

$$[e_2] = X_2 - Z_2 = \begin{bmatrix} i_{qs} - \$_{qs} \\ i_{dr} - \$_{dr} \\ i_{qr} - \$_{qr} \end{bmatrix} \tag{18}$$

Thus, the dynamics of the matrices of observation errors can be written as:

$$\left[\dot{e}_1\right] = \dot{X}_1 - \dot{Z}_1 \tag{19}$$

$$\left[\dot{e}_2\right] = \dot{X}_2 - \dot{Z}_2 \tag{20}$$

Replacing the dynamics of the real states and observed by their values, we then get:

$$\left[\dot{e}_1\right] = (A_1 - B_1) + (g_1 - h_1) - [G]sat.C_1[e_1] \tag{21}$$

$$\left[\dot{e}_2\right] = (A_2 - B_2) + (g_2 - h_2) - [K]sat.C_2[e_2] \tag{22}$$

From equations (21) and (22), it left for us to determine the matrices of the gains [G] and [K] able to ensure the stability and the global convergence of the observation errors to zero by the PSO algorithm. The interconnected observers being composed of five states, we therefore define five objectives functions for which each considered objective function is the minimization of the integral of absolute error given by the following relation:

$$J_{ITAE} = \int_0^{t_{simul}} |e_s| dt \tag{23}$$

Where tsimul is the simulation time and e_s the error between measurable and observed states.

To avoid the use of multi-objectives optimization technique, we only use one objective function defined by the following relation:

$$J = \sum_{i=1}^{5} \alpha_i J_i \tag{24}$$

$$\alpha_1 + \alpha_2 + \alpha_3 + \alpha_4 + \alpha_5 = 1 \tag{25}$$

The PSO algorithm therefore enables us to determine iteration by iteration the following values of the gains: G_1, G_2, K_1, K_2, K_3.Once the algorithm is applied, we observe its fast convergence and a weak variation of the objective function from certain iteration as depicted in Figure 4.

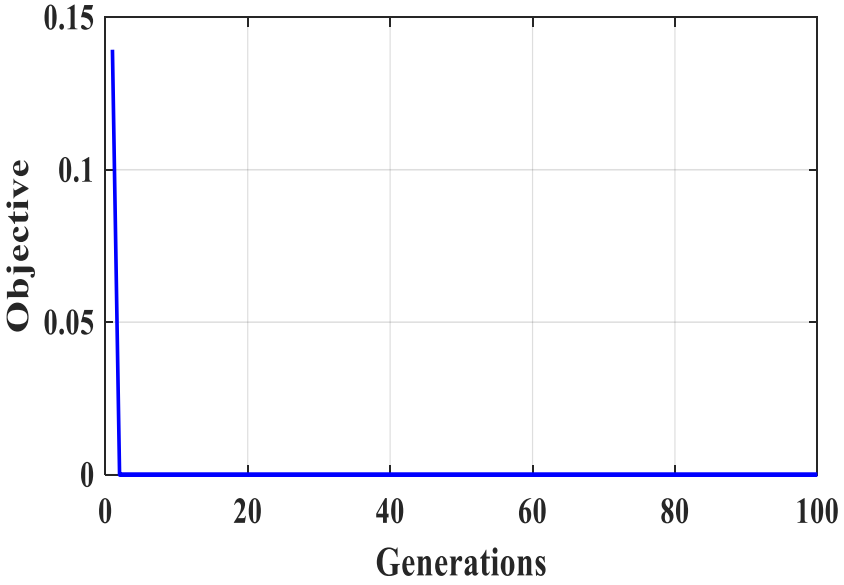

Figure 4. Objective function of the observer's gains

We can then estimate the rotor flux and electromagnetic torque of the machine depending of observed currents by the following equations:

$$\hat{\varphi}_{dr} = \hat{L}_r(i_m)\hat{i}_{dr} + \hat{M}(i_m)\hat{i}_{ds} \tag{26}$$

$$\hat{\varphi}_{qr} = \hat{L}_r(i_m)\hat{i}_{qr} + \hat{M}(i_m)\hat{i}_{qs} \tag{27}$$

$$\hat{C}_{em} = \frac{3}{2} p \hat{M}(i_m)(\hat{i}_{dr}\hat{i}_{qs} - \hat{i}_{qr}\hat{i}_{ds}) \tag{28}$$

5. Dynamic generation method of the optimal rotor flux trajectory proposed

Let's us consider the electric and magnetic equations of the induction motor in the Park frame:

$$\begin{cases} V_{ds} = R_s i_{ds} - \omega_s \varphi_{qs} + \dfrac{d\varphi_{ds}}{dt} \\ V_{qs} = R_s i_{qs} + \omega_s \varphi_{ds} + \dfrac{d\varphi_{qs}}{dt} \\ 0 = R_r i_{dr} - (\omega_s - p\Omega)\varphi_{qr} + \dfrac{d\varphi_{dr}}{dt} \\ 0 = R_r i_{qr} - (\omega_s - p\Omega)\varphi_{dr} + \dfrac{d\varphi_{qr}}{dt} \end{cases} \tag{29}$$

$$\begin{cases} \varphi_{ds} = L_s(i_m) i_{ds} + M(i_m) i_{dr} \\ \varphi_{qs} = L_s(i_m) i_{qs} + M(i_m) i_{qr} \\ \varphi_{dr} = L_r(i_m) i_{dr} + M(i_m) i_{ds} \\ \varphi_{qr} = L_r(i_m) i_{qr} + M(i_m) i_{qs} \end{cases} \quad (30)$$

Induction motors are usually designed to have maximum efficiency at their nominal operating point. However, they often operate with some fluxes different to their nominal values. In this case, it is possible to optimize the efficiency of the machine. To achieve that, the rotor flux value should be adjusted online through an algorithm for each given load and speed of the motor.

The electromagnetic torque with orientation of the rotor flux in the machine is given by the equation (31) using the equations (2) and (3):

$$C_{em} = \frac{3}{2} p \frac{M(i_m)}{L_r(i_m)} \varphi_r i_{qs} = J \frac{d\Omega}{dt} + f\Omega + Cr \quad (31)$$

Let's us consider

$$i_{qs} = \sqrt{I_s^2 - i_{ds}^2} \quad (32)$$

In the steady state, the stator current according to the direct axis becomes:

$$i_{ds} = \frac{\varphi_r}{M(i_m)} \quad (33)$$

The module of the stator's current considering the equations (31-33) is then :

$$I_s = \sqrt{\frac{C_{em}^2}{\left(1.5 p \frac{M(i_m)}{L_r(i_m)} \varphi_r\right)^2} + \left(\frac{\varphi_r}{M(i_m)}\right)^2} \quad (34)$$

For each given value of speed and the motor load, the reference of electromagnetic torque is evaluated from equation (31). For this value of electromagnetic torque, there are several combinations of the operating points (φ_{ri} , I_{si}). From the energetic point of view, only one couple (φ_r , I_s) implies a lowest stator's current. To find the best operating point, the flux φ_r is increased from 0 to 1.4 with a step of 0.01 in order to calculate the value of stator's current from equation (34). Then the value of the lowest stator's current (optimal current) as well as its index are memorized. The optimal rotor flux corresponding to the index of the optimal current previously memorized is then recovered. Thus, the best operating point (rotor flux) consuming a weak stator current is evaluated and, in that way an optimal flux trajectory is dynamically generated in real time.

6. Synthesis of the optimized sliding mode controller

From equations (29-31), the dynamics of fluxes, stator's currents and speed are calculated as below :

$$\frac{d}{dt}\varphi_{dr} = \frac{R_r}{L_r(i_m)}M(i_m)i_{ds} - \frac{R_r}{L_r(i_m)}\varphi_{dr} \tag{35}$$

$$\frac{di_{ds}}{dt} = \frac{v_{ds}}{L_s(i_m)} + \omega_s i_{qs} - \frac{R_s}{L_s(i_m)}i_{ds} + \omega_s\frac{M(i_m)}{L_s(i_m)}i_{qr} - \frac{M(i_m)}{L_s(i_m)}\frac{di_{dr}}{dt} \tag{36}$$

$$\frac{di_{qs}}{dt} = \frac{v_{qs}}{L_s(i_m)} - \omega_s i_{ds} - \frac{R_s}{L_s(i_m)}i_{qs} - \omega_s\frac{M(i_m)}{L_s(i_m)}i_{dr} - \frac{M(i_m)}{L_s(i_m)}\frac{di_{qr}}{dt} \tag{37}$$

$$\frac{d\Omega}{dt} = \frac{3}{2}\frac{pM(i_m)}{JL_r(i_m)}\varphi_r i_{qs} - \frac{f}{J}\Omega - \frac{1}{J}C_r \tag{38}$$

From these equations, we conduct the synthesis of the different sliding mode regulators.

Synthesis of the sliding mode speed regulator:

Let's us consider the mechanical equation of the speed of the machine oriented along the d axis given by equation (38).

$$i_{qst} = i_{qse} + i_{qsd} \tag{39}$$

Where i_{qse} and i_{qsd} are respectively the equivalent and discontinuous components of the control

Then, equation (38) becomes:

$$\frac{d\Omega}{dt} = \frac{3}{2}\frac{pM(i_m)}{JL_r(i_m)}\varphi_r(i_{qse} + i_{qsd}) - \frac{f}{J}\Omega - \frac{1}{J}C_r \tag{40}$$

The sliding surface of speed is defined as follows: $S_\Omega = \varepsilon_\Omega$ where $\varepsilon_\Omega = \Omega^* - \Omega$

And it dynamic becomes:

$$\dot{S}_{\Omega} = \dot{\Omega}^{*} - Ki_{qst} + c\Omega + \frac{C_r}{J} \tag{41}$$

$$\mathrm{K} = \frac{3}{2}\frac{pM(i_m)}{JL_r(i_m)}\varphi_r \quad , \quad c = \frac{f}{J}$$

Considering the invariances conditions on sliding surface ($S_{\Omega} = \dot{S}_{\Omega} = 0$) and $i_{qsd} = 0$, we obtain the following equivalent control law:

$$i_{qse} = \frac{1}{K}(f\Omega + C_r + J\dot{\Omega}^{*}) \tag{42}$$

The discontinuous component of the control can then be written as:

$$i_{qsd} = \mathrm{K}_{\Omega} sat(S_{\Omega}) \tag{43}$$

Synthesis of the sliding mode flux regulator:

Let the dynamics of the rotor flux of the machine aligned with the d axis given by equation (35).

$$i_{dst} = i_{dse} + i_{dsd} \tag{44}$$

Thus, equation (35) becomes:

$$\frac{d}{dt}\varphi_{dr} = \frac{R_r}{L_r(i_m)}M(i_m)(i_{dse} + i_{dsd}) - \frac{R_r}{L_r(i_m)}\varphi_{dr} \tag{45}$$

The sliding surface of the rotor flux is defined by: $S_{\varphi} = \varepsilon_{\varphi}$ where $\varepsilon_{\varphi} = \varphi^{*} - \varphi$

And it dynamic becomes:

$$\dot{S}_{\varphi} = \dot{\varphi}^{*} + \frac{R_r}{L_r(i_m)}\varphi_r - M(i_m)\frac{R_r}{L_r(i_m)}i_{dst} \tag{46}$$

Technium Vol. 2, Issue 6 pp.41-60 (2020)
ISSN: 2668-778X
www.techniumscience.com

Considering the invariances conditions on sliding surface ($S_\varphi = \dot{S}_\varphi = 0$) and $i_{dsd} = 0$, we obtain:

$$i_{dse} = \frac{L_r(i_m)}{R_r M(i_m)}(\dot{\varphi}^* + \frac{R_r}{L_r(i_m)}\varphi_r) \tag{47}$$

The discontinuous component of the flux control can then be written as:

$$i_{dsd} = \mathrm{K}_\varphi sat(S_\varphi) \tag{48}$$

Calculation of the sliding mode current ids regulator:

Equation (36) give the ids current of the sliding mode regulator. Assume that the control tension is:

$$v_{dst} = v_{dse} + v_{dsd} \tag{49}$$

And the sliding surface of this current defined by: $S_{i_{ds}} = \varepsilon_{i_{ds}}$ where $\varepsilon_\varphi = i_{ds}^* - i_{ds}$

Thus, the dynamic of this sliding surface becomes:

$$\dot{S}_{i_{ds}} = \dot{i}_{ds}^* - \frac{(v_{dse} + v_{dsd})}{L_s(i_m)} - \omega_s i_{qs} + \frac{R_s}{L_s(i_m)} i_{ds} - \omega_s \frac{M(i_m)}{L_s(i_m)} i_{qr} + \frac{M(i_m)}{L_s(i_m)} \frac{di_{dr}}{dt} \tag{50}$$

Considering the invariance conditions on sliding surface ($S_{i_{ds}} = \dot{S}_{i_{ds}} = 0$) and $v_{dsd} = 0$, we obtain:

$$v_{dse} = L_s(i_m)\dot{i}_{ds}^* - L_s(i_m)\omega_s i_{qs} + R_s i_{ds} - \omega_s M(i_m) i_{qr} + M(i_m)\frac{di_{dr}}{dt} \tag{51}$$

The discontinuous component of the control tension is then:

$$v_{dsd} = \mathrm{K}_{i_{ds}} sat(S_{i_{ds}}) \tag{52}$$

Calculation of sliding mode current *iqs* regulator:

The *iqs* current of the sliding mode regulator is given by equation (37). Assume that the control tension is:

$$v_{qst} = v_{qse} + v_{qsd} \tag{53}$$

And the current sliding surface defined by: $S_{i_{qs}} = \varepsilon_{i_{qs}}$ where $\varepsilon_{\varphi} = \dot{i}_{qs}^{*} - i_{qs}$

Thus, the dynamic of this sliding surface becomes:

$$\dot{S}_{i_{ds}} = \dot{i}_{qs}^{*} - \frac{(v_{qse} + v_{qsd})}{L_s(i_m)} + \omega_s i_{ds} + \frac{R_s}{L_s(i_m)} i_{qs} + \omega_s \frac{M(i_m)}{L_s(i_m)} i_{dr} + \frac{M(i_m)}{L_s(i_m)} \frac{di_{qr}}{dt} \tag{54}$$

Considering the invariance conditions on sliding surface, ($S_{i_{qs}} = \dot{S}_{i_{qs}} = 0$) and $v_{qsd} = 0$, we obtain:

$$v_{qse} = L_s(i_m)\dot{i}_{qs}^{*} + L_s(i_m)\omega_s i_{ds} + R_s i_{qs} + \omega_s M(i_m) i_{dr} + M(i_m)\frac{di_{qr}}{dt} \tag{55}$$

The discontinuous component of the control tension is then:

$$v_{qsd} = K_{i_{qs}} sat(S_{i_{qs}}) \tag{56}$$

7. Synthesis of different regulators using particle swarm optimization

The optimization of the sliding mode regulators is also done using the PSO algorithm. Here, four objectives functions are defined: the minimization of the integral of the absolute error of speed, of the rotor flux, and both stator currents. However, the formulation of only one objective function that uses the method of level-headedness as presented in the case of the observers is done. This optimization algorithm determines the good values of parameters that minimize the global criteria J.

The objective function that shows the convergence and the stability of the method is given in Figure 5 below

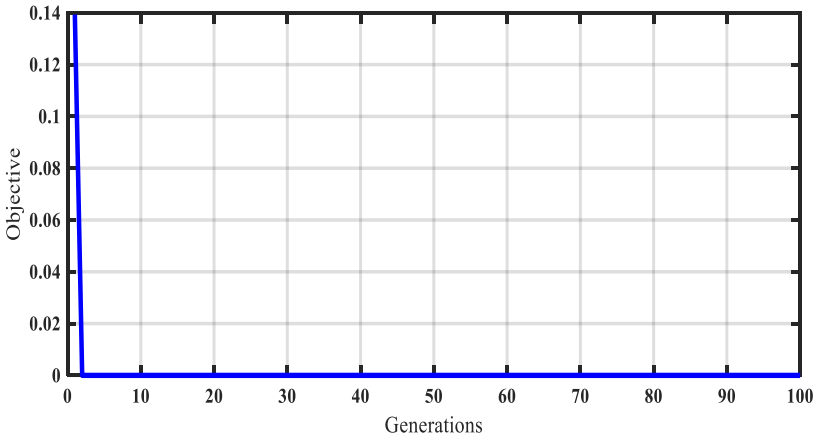

Figure 5. Objective function of sliding mode regulators

The induction motor with sensorless controller is simulated in the Matlab/Simulink environment using the electromechanical characteristics of a real-life machine given by [16]. It is a 36 kW induction machine whose magnetic characteristic is considered. The references of the speed and load consider all trajectories that allow us to analyze and illustrate the dynamic performances of the sensorless controller. The initial values of the mechanical speed and the load are maintained to 0 to allow the flux to settle in the machine.

At t=0.75s, the speed of the machine is carried to 20 rad/s and remains constant until 5 s. A load (Figure 6) of three different levels is applied between 1s and 4.5s. This first phase permits us to test and to evaluate the dynamic performances of the sensorless controller in low speed with load. The machine is then accelerated until a high speed (100 rad/s). Then between t=6.5s and 9.5s, three increasing level loads are applied again. The objective of this second phase is to test the performances of the sensorless control during a big transient of speed and in high speed with load. Then, the machine is slowed down quickly to reach at t=12s, a negative weak speed (-1 rad/s) that will remain constant until t=15s with load. This phase shows the performance of the sensorless induction motor in the critical zone so-called “unobservable”. Finally, the trajectories bring the machine in the low speed zone.

Figure 7 generated dynamically using the developed algorithm for each value of the speed and the load, shows a trajectory of the optimal flux allowing optimizing the energy of the machine.

Figure 8 and Figure 9 show the results of simulation in the case of the nominal resistances. One can notice some good dynamic performances in terms of tracking trajectory and disturbance rejection. In terms of tracking trajectory, the observed speed converges correctly towards its reference (speed, precision and stability) even in the critical zone. There is the same conclusion for the tracking of the flux. In terms of disturbance rejection, one can notice on Figure 8 that the load is very rejected in high speed, in low speed and in very low speed (critical zone).

Figure 10 shows the module of the stator absorbed current for a variable flux and Figure 11 shows the case of stationary flux. In all operating condition, the sensorless control with variable flux reference (magnetic saturation) absorbs a weaker current. This difference is more meaningful with a weak load.

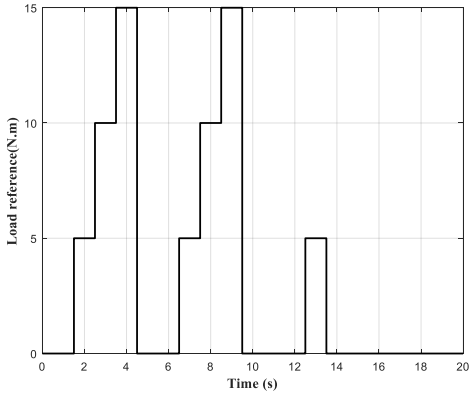

Figure 6. Load torque reference

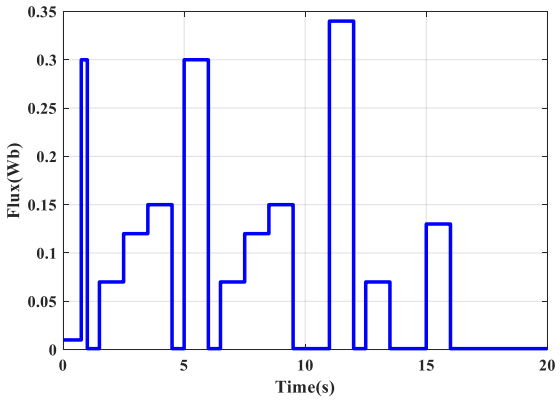

Figure 7. Optimal rotor flux dynamically generated

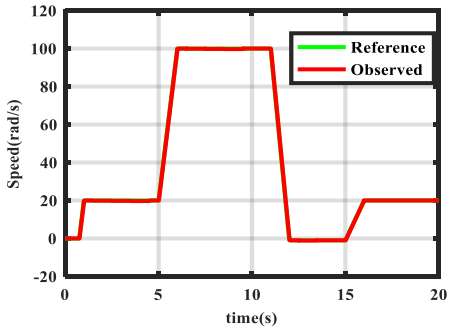

Figure 8. Speed reference and observed

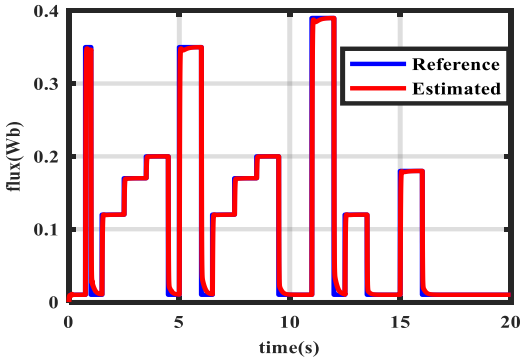

Figure 9. Estimation of Rotor flux

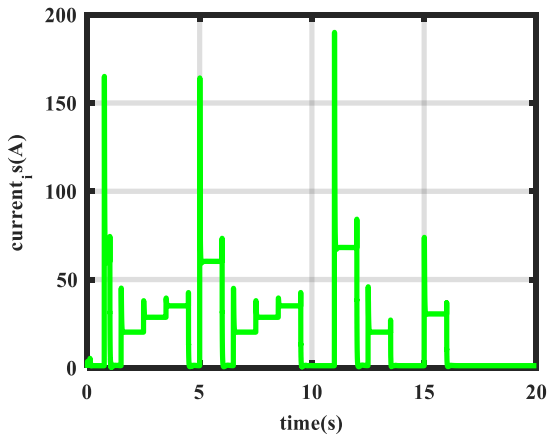

Figure 10. Stator module current for variable flux

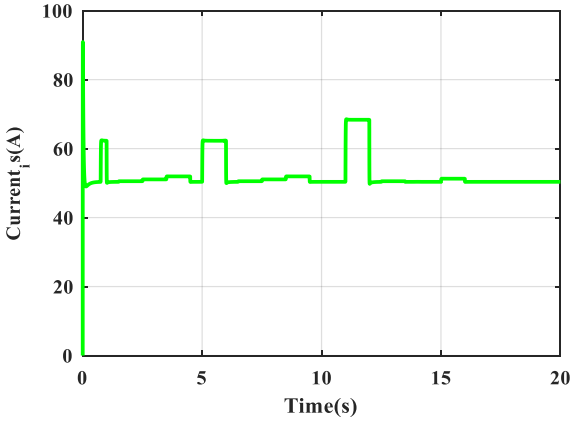

Figure 11. Stator module current for constant flux

Analysis of the robustness:

For the robustness tests, we respectively vary the resistors values of the observers and the controller. The inductances already vary according to the level of saturation. In this purpose, Figure 12, Figure 13, Figure 14 and Figure 15 show the results respectively for a variation of -50% and +50% on the nominal value of the stator resistance. Figure 16, Figure 17, Figure 18 and Figure 19 show the results respectively for a variation of -50% and +50% of the nominal value of the rotor resistance. For all these variations, one can notice an insensitivity of the speed. But, flux is weakly sensitive. However, one can globally tell that, the results are identical to those got with the nominal values.

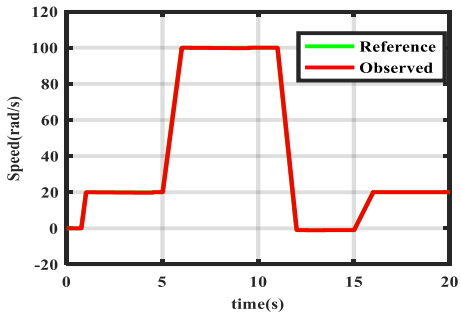

Figure 12. Speed robustness at -50% on Rs

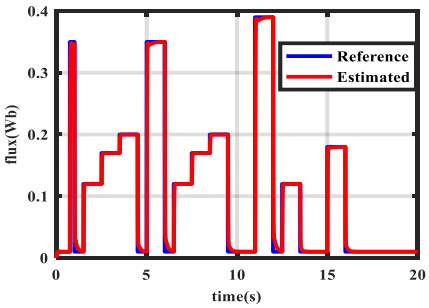

Figure 13. Flux robustness at -50% on Rs

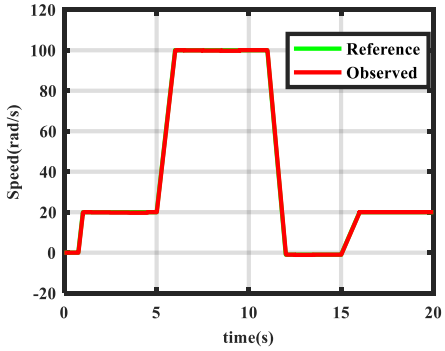

Figure 14. Speed robustness at +50% on Rs

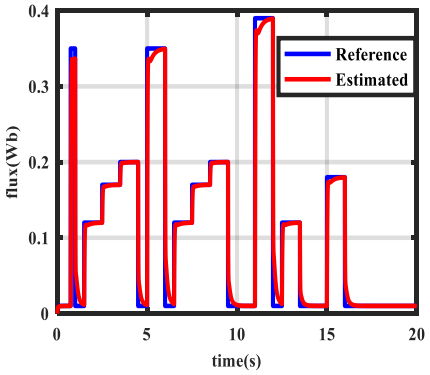

Figure 15. Flux robustness at +50% on Rs

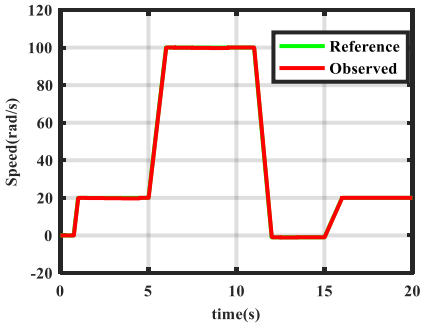

Figure 16. Speed robustness at -50% on Rr

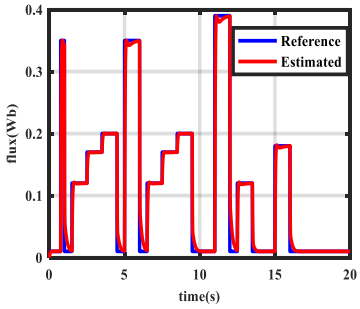

Figure 17. Flux robustness at -50% on Rr

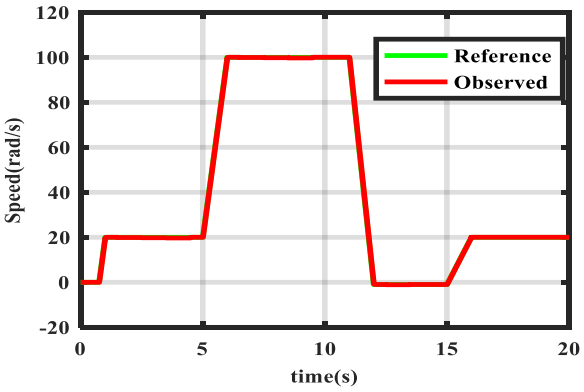

Figure 18. Speed robustness at +50% on Rr

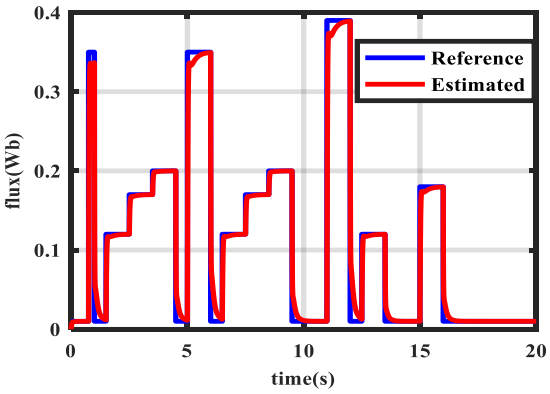

Figure 19. Flux robustness at +50% on Rr

Comparing these results with those of [7], it appears that, the tracking trajectory, the robustness and the energy optimization are apparently equivalents. However, the fast convergence and better minimization of objectives functions to the inaccurate model considered, the fast-computational times, and the simplicity to practical implementation by power electronics converters make this control strategy more suitable. The traditional chattering phenomenon of the sensorless sliding mode control, which is present in several recent papers, is eliminated here.

8. Conclusion

In this article, a double optimization of the sensorless sliding mode control of induction motor considering the magnetic saturation is proposed. Interconnected sliding mode observers are used to replace speed, rotor currents and flux sensors. We determine the optimal gains of the observers and the optimal parameters of the sliding regulators by using particle swarm optimization algorithm. An energy optimization algorithm is developed. The obtained results show effective energy optimization and some good dynamic performances (tracking trajectory, disturbance rejection, elimination of chattering phenomenon, global stability and convergence of the system in all operating range of the machine even in the critical zone called unobservable). These results show the efficiency of the proposed control strategy. In the forthcoming paper, we plan to experimentally realize the proposed control scheme.

References

[1] B. Abderrahim, B. Sandeep, J. Mustapha, E. Adil, and A. Mohammed : Real time high performance of sliding mode-controlled induction motor drives , Procedia computer science, Vol.132, pp.971-982, 2018.

[2] E. Abderrahim, G. Fouad, E. M. Abdelmounime, L. Rachid, and Z. C. Fatima: Adaptative control strategy with flux reference optimization for sensorless induction motors, Control Engineering Practice, Vol. 26, pp.91-106, 2014.

[3] T. Ameid, A Menacer, H. Talhaoui, Harzelli, and A Ammar: Simulation and real-time implementation of sensorless field-oriented control of induction motor at healthy state using rotor cage model and EKF, In 2016 IEEE 8th International Conference on Modelling, Identification and Control (ICMIC) ,2016. DOI: 10.1109/ICMIC.2016.7804201.

[4] I. Benlaloui, S. Drid, Chifri-Alaoui, and M. Ouriagli: Implementation of a new MRAS speed sensorless vector control of induction machine, IEEE Transactions on Energy conversion, vol.30, no.2, pp.588-595, 2015.

[5] M. J. Elmano, F. José, M. Resende, and P. Joao : A new control strategy with saturation effect compensation for an autonomous induction generator driven by wide speed range turbines, Energy conversion and Management, Vol.52, No.5, pp.2142-2152, 2011.
[6] S. E. F. Fares, M. Omar, and A. E. Wejdan : D-Q model and control of a three-phase induction motor considering mutual flux saturation effect, In 2017 IEEE 10th Jordan International Electrical and Electronics Engineering Conference (JIEEEC), 2017. DOI: 10.1109/JIEEEC.2017.8051400
[7] F. Hiswe, J. Y. Effa, and F. E. D. Kenmoe : Optimization of sensorless field-oriented control of an induction motor taking into account of magnetic saturation, International Journal of Dynamics and Control. DOI 10.1007/s40435-018-00503-8. 2019.
[8] J. Hong, S. Laflamme, L. Cao, B. Joyce, and J. Dodson : Hybrid algorithm for structural health monitoring of high-rate systems, In ASME 2018 Conference on Smart Materials, Adaptive Structures and Intelligent Systems. https://doi.org/10.1115/SMASIS2018-7977, 2018.
[9] J. Kennedy, and R. Eberhart : Particle swarm optimization, In Proceedings of ICNN'95 - International Conference on Neural Networks, No.4, pp.1942-1948, 1995. DOI: 10.1109/ICNN.1995.488968.
[10] A. Keyhani, and H. Tsai: IGSPICE simulation of induction Machines with saturable inductances, IEEE Transactions on Energy conversion, Vol.4, No.1, pp.118-125, 1989.
[11] S. Lavanyas, A.J. Mohamed, K. P. Suresh, V. Vijayalakshmi, and R. J. Jenifer: A sensorless sliding mode control-based induction motor drive for industrial application, International Journal of Engineering Research and General science, Vol.4, No.2, pp. 764-777, 2016.
[12] R. D. Lorenz, and D.W. Novotny : Saturation effects in field-oriented induction machines, IEEE Transactions on Industry Applications, Vol.26, No.2, pp.283-289, 1990.
[13] L. Lu, D. Xudond, and S. Shuiwen : Indirect field-oriented control torque of induction motor considering magnetic saturation effects: errors analysis , IET Electric Power Applications, Vol.11, No.6, pp.1105-1113,2017.
[14] S. Mona: Speed sensorless induction motors drive system using particle swarm optimization, International Journal of Industrial Electronics and Drives, Vol.2, No.4, pp.226-233, 2015.
[15] M. H. Moradi, and P. G. Khorazani : A new Matlab simulation of induction Motor, In IEEE 2008 Australasian Universities Power Engineering Conference, 2008.
[16] O. Okoro: MATLAB simulation of an induction machine with saturable leakage and magnetizing inductances,Pacific Journal of Science and Technology, Vol.5, No.1, pp. 5-15, 2004.
[17] K. Oleh, M. Bodson, and J. Wang: Comparison of two magnetic saturation of induction machines and experimental validation, IEEE Transactions on Industrial Electronics, Vol.64, No.1, pp. 81-90. , 2017.
[18] H. Ouadi, F. G. Giri, A. Elfadili, and L. Dugard: Induction machine speed control with flux optimization, Control Engineering Practice, Vol.1, No.18, pp.55-66, 2010.
[19] R. T. Novotnak, J. Chiasson, and M. Bedson : High performance motion control of an induction motor with magnetic saturation, IEEE Transactions on Control Systems Technology, Vol.7, No.3, pp.315-327, 1999.
[20] Y. Zhang, Z. Zhengming, L. Ting, Y. Liqiang, X. Wei, and Z. Jianguo : comparative study of Luenberger observer, sliding mode observer and extended Kalman filter for sensorless vector control of induction motor drives," In 2009 IEEE Energy Conversion Congress and Exposition, pp.2466-2473, 2009. A DOI: 10.1109/ECCE.2009.5316508.